Optimization and Design of a 48-to-12 V, 35 A Split-Phase Dickson Switched-Capacitor Converter

2021 IEEE Applied Power Electronics Conference and Exposition (APEC) | 978-1-7281-8949-9/21/$31.00 ©2021 IEEE | DOI: 10.1109/APEC42165.2021.9487333

Richard (Yue) Sun, Samuel Webb, *Student Member, IEEE*, Yan-Fei Liu, *Fellow, IEEE,* Paresh C. Sen, *Fellow, IEEE*
Department of Electrical and Computer Engineering, Queen's University
Kingston, Ontario, Canada, K7L 3N6
sun.richard@queensu.ca, sam.webb@queensu.ca, yanfei.liu@queensu.ca, senp@queensu.ca

***Abstract* – The switched-capacitor converter (SCC) topology has been gaining attention in recent years because of their advantages of higher power density, switch utilization, and reduced component stress compared to existing converter topologies. However, SCCs have a major drawback in which capacitor charge redistribution results in significant current spikes. One method of addressing charge redistribution is split-phase operation, which accomplishes this by imposing voltage control on the SCC's flying capacitors. However, an important design consideration was identified regarding the implementation of the split-phase Dickson SCC in high-current applications. Mismatched flying capacitors exhibit uneven charge rates, resulting in incomplete elimination of charge redistribution by split-phase control. This paper presents a discussion of the effects of mismatched flying capacitors on the operation of the split-phase Dickson SCC. Furthermore, design processes and test results of a prototype high-current split-phase Dickson SCC will be presented.**

***Keywords* – Switched-Capacitor converter, Dickson converter, Split-Phase Control, Capacitor Mismatch**

I. INTRODUCTION

In response to the ever-increasing power demands of data centers, many next-generation power architectures that promise reductions in conversion and distribution losses, such as the 48 V power architecture [1], have been developed in recent years. However, with the need to bridge the gaps between these next-generation power infrastructures with the existing 12 V infrastructure, the advantages of these next generation power architectures cannot be fully realized with existing inductor-based power converter topologies, which are typically underperforming and bulky [2] [3]. For this reason, Switched-Capacitor converters (SCC), has been gaining increased attention with researchers because of their properties of increased power density [4] [5], reduced reliance on magnetic components [6], lower component stress [7] [8], increased switch utilization [9], and simple control [10]. However, a major drawback with SCCs is that they experience charge redistribution [6]. This occurs when two capacitors with unequal voltages are suddenly connected in parallel, giving rise to significant current spikes [11] [12], and contributing both to power losses [13] [14] [15] [16] and potential component failure. This drawback has precluded the implementation of the switched-capacitor converter outside of low-current applications with no more than 10 A [14] [15] [17] [18]. While measures such as large flying capacitors [19] and high switching frequencies can partially offset the effects of charge redistribution, enabling implementation in higher-current applications, they compromise power density, converter performance, and/or efficiency, in addition to introducing other problems such as electromagnetic interference [20].

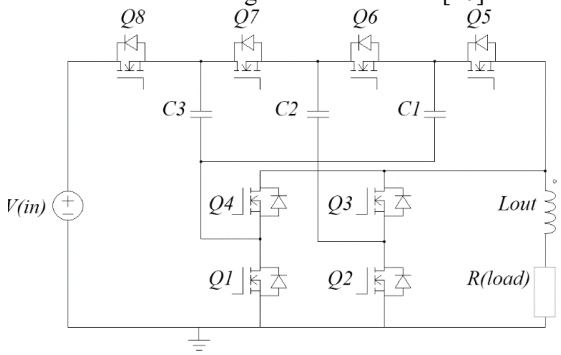

Figure 1: 4-to-1 step-down Dickson SC converter schematic

One method of overcoming charge redistribution within the Dickson SCC topology (Figure 1), is split-phase control [17]. SCCs are typically operated with 50% duty cycles on all switches. However, in two-phase operation, there are large voltage differences between the equivalent circuits during switching, resulting in significant charge redistribution. By imposing lower duty cycles on some of the switches, the charging and discharging of the flying capacitors can be controlled, enabling the equalization of the branch voltage before switching takes place. Split-phase operation therefore significantly reduces the drawback of charge redistribution, allowing the Dickson SCC to be implemented in high-current applications without utilizing large components or high-speed switching.

A critical design consideration for the high-current split-phase Dickson SCC is the need for flying capacitor matching. Since split-phase control effectively relies on charging/discharging control of flying capacitors to compensate for charge redistribution, uneven charging and discharging due to mismatch between the flying capacitors can result in branch voltage differences during switching. Split-phase control therefore cannot fully eliminate charge redistribution in this operating condition without adding

significant additional control. Therefore, it is crucial that mismatch between the flying capacitors is kept as minimal as possible.

To increase the SCC's power density and performance, ceramic capacitors are the capacitor of choice for construction of the flying capacitors. However, their inherent property of DC voltage de-rating, manufacturing tolerance, and fact that each flying capacitor will have a different DC bias voltage in operation, makes perfect matching of the flying capacitors difficult.

A prototype of the 48 V to 12 V, 35 A was able to attain a full-load efficiency of 96.3% at 12V/35A operating conditions. During prototype testing, the high-current split-phase Dickson SCC prototype was shown to perform satisfactorily with both matched flying capacitors, as well as with flying capacitors mismatched by up to 30% from nominal. Comparing the two operating conditions, operation with matched flying capacitors resulted in improved efficiency and decreased overall temperatures.

The structure of the remainder of the paper is as follows: A topology overview of both two-phase and split-phase operation is presented in Section II, the impact of flying capacitor mismatch on split-phase operation is presented in Section III, Section IV presents design methodologies for the high-current split-phase Dickson SCC prototype, and the derivation of an in-circuit capacitance measurement method. Finally, the findings from prototype testing of a high-current 4-to-1 split-phase Dickson SCC prototype are presented in Section V.

II. Overview of Topology and Split-phase Control

Switched-Capacitor converters are usually operated with 50% duty cycles on all switches. A 4-to-1 step-down Dickson SCC (Figure 1) operates with half its switches (Q8, 6, 4, and 2) conducting during Phase 1, and with its remaining switches (Q7, 5, 3, and 1) conducting during Phase 2. Two-phase operation results in two equivalent circuits, as shown in Figure 2 [17].

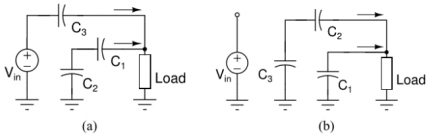

Figure 2: Two-phase equivalent circuits of 4-to-1 Dickson Converter [17]

As previously discussed, a major drawback of SCCs is charge redistribution, which occurs when two capacitors (or capacitive branches) with unequal voltages are suddenly connected in parallel. As shown in Figure 3, when two-phase operation was simulated with a high-current load, voltage differences of nearly 2 V were observed between the equivalent circuit branches during switching. The resulting charge redistribution produced current spikes of up to 300 A. These current spikes in practice will result in drastically increased switching and conduction losses, as well as the risk of component failure. Refer to Table 1 for the simulation parameters.

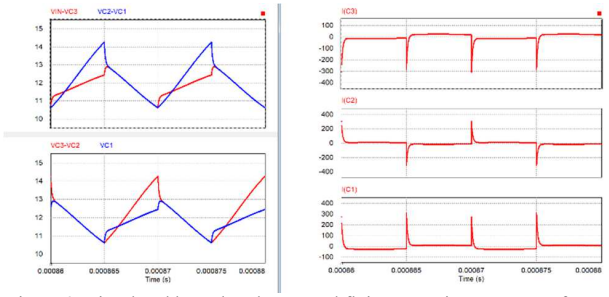

Figure 3: Simulated branch voltages and flying capacitor currents of Two-phase 4-to-1 Dickson Converter. Refer to Table 1 for simulation parameters.

TABLE 1. Simulation Parameters

Input Voltage, V_{IN}	**48 V**
Output Current, I_{OUT}	**35 A**
Flying Capacitor Sizes, C_3, C_2, C_1 (nominal)	**47 µF**
Output Capacitor Size, C_{OUT}	**47 µF**
Output Inductor Size, L_{OUT}	**200 nH**
Switching Frequency, f_{SW}	**100 kHz**
MOSFET On-Resistance, $R_{DS(on)}$	**1 mΩ**
Flying Capacitor Equivalent Series Resistance, R_{ESR}	**1 mΩ**

As shown in Figure 3, two-phase operation of a high-current SCC produces current spikes of unacceptable magnitudes. Instead of alleviating charge redistribution using large components or increased switching frequencies (which may lead to other compromises), another approach is to ensure that the voltages of the equivalent circuits line up before switching takes place by turning off some switches earlier than other switches they operate in phase with, in effect controlling the charging and discharging of the flying capacitors.

Split-phase control [17] is one such method of imposing charge/discharge control on the flying capacitors through imposing lower duty cycles on some switches. The switches with reduced duty cycles imposed are typically those that conduct within equivalent circuit branches consisting of a single flying capacitor. In a 4-to-1 Dickson SCC, these switches are Q8 and Q5. The duty cycles to be imposed on these 'split-phase' switches are dependent on the circuit's conversion ratio [17]. Using Equation 1 [17], the duty cycles to be imposed on switches Q8 and Q5 to realize split-phase operation is 37.5%. As shown in Figure 4 [17], split-phase operation of the 4-to-1 Dickson SCC results in 4 equivalent circuits.

$$D_{(split-phase)} = \frac{N+2}{4N} \tag{1}$$

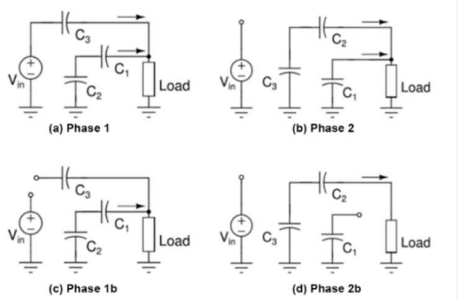

Figure 4: Split-phase equivalent circuits of 4-to-1 Dickson Converter [17]

Phases 1b and 2b are the additional circuit states resulting from the implementation of split-phase operation of the 4-to-1 Dickson SCC. As shown in Figures 4c (Phase 1b) and Figure 4d (Phase 2b), capacitors C1 and C3 are periodically disconnected from the circuit during Phases 1b and 2b. As a result, the charging behavior of C1 and C3 are directly controlled by split-phase control, while the periodic removal of one circuit branch during Phases 1b and 2b indirectly controls the charging and discharging rates of the other flying capacitors. With the voltage balancing between the circuit branches during Phases 1b and 2b, branch voltage differences can be significantly reduced, allowing switching to take place with little to no current transients.

A small inductor is required in front of the load in order to ensure that current continues to flow to the load throughout the switching cycle [14] [15] [17].

A simulation of split-phase operation (Figure 5) with the same load and circuit characteristics shown in Table 1 shows that the additional charging/discharging control provided by split-phase control resulted in significantly reduced differences in branch voltages during switching. Consequently, charge redistribution is also reduced.

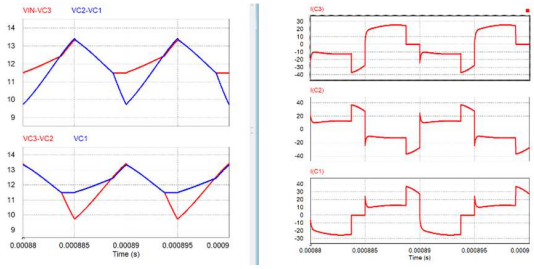

Figure 5: Simulated branch voltage and flying capacitor currents of Split-phase 4-to-1 Dickson Converter. Refer to Table 1 for simulation parameters.

With charge redistribution significantly reduced, the performance of the Dickson SCC is improved, thanks to the reduction of conduction and switching losses compared to two-phase operation. Additionally, the charge/discharge control provided by split-phase operation allows the Dickson SCC to be implemented in high-current applications using smaller flying capacitors, improving the converter's power density.

III. Simulations and Analysis of Flying Capacitor Mismatch

By reducing charge redistribution significantly, split-phase control allows for feasible implementation of the Dickson SC converter in high-current applications. However, no prior high-current implementations of the split-phase Dickson SCC have been reported. Therefore, an analysis of practical factors and implications would be necessary to successfully adapt the split-phase Dickson SCC for effective operation in the 48 V to 12 V, 35 A operating condition.

The derivations for split-phase operation [17] were made with the assumption that perfect matching of capacitances existed between the flying capacitors of the Dickson SCC. Split-phase operation relies on charge/discharge control of the flying capacitors to mitigate the effects of charge redistribution within the Dickson SCC. If there is mismatch in capacitance between the Dickson SCC's flying capacitors, they do not charge and discharge evenly. The hard-wired nature of the duty cycles under split-phase control means that without added control complexity, voltage differences between the equivalent circuit branches will be present during switching, consequently resulting in incomplete compensation of charge redistribution under split-phase control.

To analyze the impact of mismatched flying capacitors on split-phase operation of the Dickson SCC, various simulations were carried out on the 4-to-1 split-phase Dickson SCC topology, using circuit parameters tabulated in Table 1. To reflect typical manufacturing tolerances of electronic components, the capacitances of the individual flying capacitors were varied by ±20% throughout the simulations. Simulation results from a scenario where the capacitance of one of the flying capacitors, C3, was varied by -20% compared to the remaining flying capacitors, are shown in Figure 6.

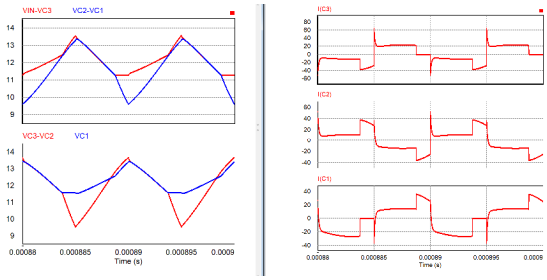

Figure 6: Simulated equivalent circuit branch voltage waveforms and flying capacitor currents for 4-to-1 split-phase Dickson SCC, with variance of -20% on C3.

Compared to the ideal scenario presented in Figure 5, when C3 had its capacitance reduced by 20%, voltage differences of around 0.27 V were observed during both switching transitions. This resulted in current spikes of a maximum of 60 A through the flying capacitors. Further simulations were performed with capacitance variations on other flying capacitors; the flying capacitor values and maximum currents observed through each capacitor for each simulated scenario are tabulated in Table 2.

TABLE 2. Summary of Capacitor Mismatch Analysis Simulations – Maximum Capacitor Currents

Scenario	C3 size (µF)	C2 size (µF)	C1 size (µF)	IC3 (A, max)	IC2 (A, max)	IC1 (A, max)
Ideal	47.00	47.00	47.00	36.89	36.89	36.87
C3 -20%	37.60	47.00	47.00	64.14	52.30	36.29
C3 +20%	56.40	47.00	47.00	35.99	62.31	62.31
C2 -20%	47.00	37.60	47.00	62.66	62.86	62.86
C2 +20%	47.00	56.40	47.00	36.71	36.71	36.69
C1 -20%	47.00	47.00	37.60	36.47	52.50	64.30
C1 +20%	47.00	47.00	56.40	62.02	62.02	35.97

As shown in Table 2, almost all single-capacitor variance scenarios resulted in significant charge redistribution between the flying capacitors, clearly indicating that split-phase operation is sensitive to mismatches between the flying capacitors. The only simulated scenario of flying capacitor variance that did not result in significant charge redistribution

was when the capacitance of flying capacitor C2 was increased by 20%. Figure 7 shows the simulated voltage and current waveforms of this operating scenario.

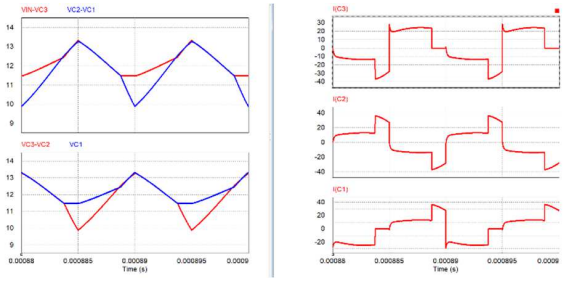

Figure 7: Simulated equivalent circuit branch voltage waveforms and flying capacitor currents for 4-to-1 split-phase Dickson SCC, with variance of +20% on C2.

Referring to the simulation results from the ideal scenario (Figure 5), the voltages of the circuit branches containing capacitor C2 were slightly higher than the voltages of the other circuit branches during both switching transitions. An increase in the capacitance of C2 meant that it experienced less voltage ripple. Correspondingly, compared to the ideal waveforms shown in Figure 5, branch voltage waveforms ($V_{C2} - V_{C1}$) during Phase 1 transition, and ($V_{C3} - V_{C2}$) during Phase 2 transition, were shifted downwards during switching, reducing the magnitudes of the voltage differences during switching in this scenario.

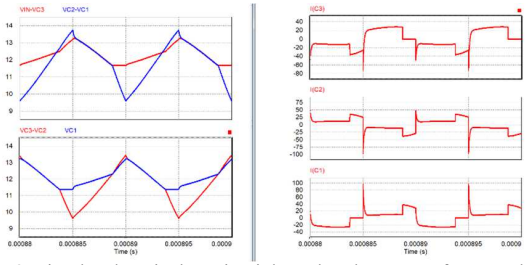

Figure 8: Simulated equivalent circuit branch voltage waveforms and flying capacitor currents for 4-to-1 split-phase Dickson SCC. All flying capacitors mismatched.

When the capacitances of every flying capacitor are different from each other, the resulting voltage differences and current spikes can be significantly increased compared to scenarios with variance on only one flying capacitor. The voltage and current waveforms of such a scenario are presented in Figure 8. For this simulated scenario, C3's capacitance was set to 56.4 µF, C2 was set to 37.6 µF, C1 was set to 47 µF. As shown in Figure 8, operation with completely mismatched flying capacitors resulted in current spikes of nearly 100 A, highlighting the effect of flying capacitor mismatch on split-phase operation.

It has previously been established in the discussions in Section II that charge redistribution results in increased switching and conduction losses, as well as increased chances of component failure. Therefore, it can be concluded from this simulation analysis that the flying capacitors of the split-phase Dickson SCC should be designed such that mismatch between them is minimized. However, this design consideration ideally requires precise capacitors. Practical characteristics of capacitors, as well as manufacturing tolerance, may cause the values of the flying capacitors to be different from each other in operation.

IV. Prototype Design and Considerations

The analysis from simulations regarding flying capacitor mismatch established that the ideal operating condition for the split-phase Dickson SCC is when no mismatch is present between the flying capacitors. To minimize losses due to capacitor ESR and maximize power density, switched-capacitor converters are typically constructed with ceramic capacitors. Ceramic capacitors, however, are known to lose capacitance in the presence of a DC bias voltage. This de-rating characteristic of ceramic capacitors is therefore an important consideration in matching the flying capacitors for the split-phase Dickson SCC.

TABLE 3. Flying Capacitor Values and Quantities Used for Prototype, Based on De-rating

Capacitor size and nominal capacitance	Expected DC bias voltage	Expected de-rating at DC bias	Per-unit capacitance at expected DC bias	Units needed for 60µF
1210, 4.7 µF (Capacitor C3)	36 V	-57%	2.02 µF	30
1210, 10 µF (Capacitor C2)	24 V	-42%	5.8 µF	10
1206, 10 µF (Capacitor C1)	12 V	-40%	6 µF	10

An in-operation value of 60 µF was selected for the flying capacitors of the 48 V to 12 V, 35 A split-phase Dickson SCC prototype. For comparison, the two-phase 48 V to 12 V example shown in [19] used flying capacitors as large as 500 µF. The components used to construct the three flying capacitors of the 4-to-1 prototype are shown in Table 3. Each flying capacitor array was designed based on the de-ratings of the ceramic capacitors at their expected DC blocking voltages in operation.

Along with ceramic capacitor de-rating, manufacturing tolerance (typically ±20%) is another potential source of mismatch between the flying capacitors. Because prediction of component variance due to manufacturing tolerance is difficult, as well as the part-to-part variance in the de-rating curves of the ceramic capacitors, an in-circuit estimation method was developed to estimate the actual flying capacitor sizes based on their voltage waveforms. Using this method, the values of the flying capacitors can be verified in operation and would further allow for tuning of the flying capacitors if needed. The derivation of the in-circuit estimation method is described in detail in the following subsection. An example using one of the voltage waveforms obtained from prototype testing is also provided to demonstrate the method.

A. Derivation of In-Circuit Capacitance Estimation Method

The simulation analysis presented in Section III established that mismatch between the flying capacitors of the split-phase

Dickson SCC should be kept as minimal as possible. To ensure that flying capacitor mismatch be kept to a minimum, the expected and actual de-ratings of the flying capacitors should be as close to each other as possible.

As discussed in Section II, split-phase operation produces four equivalent circuits. Two of these equivalent circuits (Phases 1b and 2b; Figures 4c and 4d [17]) are sub-phases resulting from the application of split-phase control to the circuit [17]. Both the Phase 1b and Phase 2b equivalent circuits consist of a single circuit branch consisting of two flying capacitors and the load in serial connection. Since the output inductor will ensure the load current remains approximately constant during Phases 1b and 2b, the components comprising Phase 1b and Phase 2b equivalent circuits carry the full load current for the duration of these circuit phases.

The equivalent circuit diagrams presented in Figure 4 (see Section II) show that each flying capacitor is active in at least one of either Phase 1b or 2b per switching cycle (capacitors C2 and C1 are connected in series with the load during Phase 1b, and capacitors C3 and C2 are connected in series with the load during Phase 2b). Since the load current is a known value, first principles can be used in conjunction with the flying capacitors' voltage waveforms to obtain their in-operation values, and therefore allow comparison of their actual and expected de-ratings. The time intervals where the flying capacitors carry the full load current can be identified by instances where the slope of the voltage waveforms are the steepest.

Figure 9: Magnified voltage waveform of C3, centered around the instance where it is carrying full load current.

As an example, Figure 9, obtained from prototype testing, shows the magnified waveform of capacitor C3 at the instance where it is carrying the full output current (highlighted by the red line). The voltage of capacitor C3 changed by 1.9 vertical divisions over a period of 2.6 horizontal divisions. With scales of 250 mV per vertical division and 400 ns per horizontal division, C3 experienced a change in voltage of 0.45 V over 1.04 µs. The real capacitance of C3, as calculated through Equation 2 using the information obtained from the voltage waveform, along with the load current of 35 A, was 78.7 µF.

$$C = I_{Load} * \frac{\Delta t}{\Delta V} \qquad (2)$$

B. Other circuit components

It is expected that switches Q6 and Q7 would need to block a maximum of ½ V_{IN}, while all other switches are expected to block a maximum of ¼ V_{IN}. Table 4 shows other components used to construct the power stage of the 48-to-12 V split-phase Dickson converter.

TABLE 4. OTHER PROTOTYPE COMPONENTS

Component	Manufacturer Part #	Number Required
MOSFET (25V rating)	SIRC16DP-T1-GE3	6
MOSFET (40V rating)	BSC010N04LSI	2
Inductor (200 nH)	PA3790.201HL	1
Capacitor (2200 µF)	63ZLH2200MEFC18X40	1

A 2200 µF electrolytic capacitor was used because it was discovered that input voltage ripple could compromise the effectiveness of split-phase control. Since the input source is in series with capacitor C3 during Phase 1, any input voltage ripple will appear as a difference in branch voltages at the time of switching which is not compensated for by split-phase control. As the size of the input capacitor is increased, the input voltage ripple is suppressed. Since the main objective of prototype testing was to verify that the split-phase Dickson converter could be adapted for use in high-current applications, it was therefore decided to eliminate input voltage ripple using the 2200 µF electrolytic input capacitor.

The completed prototype measures approximately 2 inches by 2 inches, with the power stage taking up 1.125-inches by 1.563-inches. Figures 10 and 11 show the top and bottom views of the power stage of the prototype. With a thickness of 0.5 inches, the power stage takes up a volume of 0.88 in^3. The maximum output power is 420 W; this gives a power density of 477 W/in^3. It operates with a switching frequency of 100 kHz.

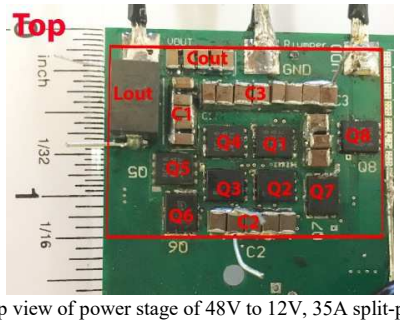

Figure 10: Top view of power stage of 48V to 12V, 35A split-phase Dickson SCC prototype. Control components and input capacitor not shown

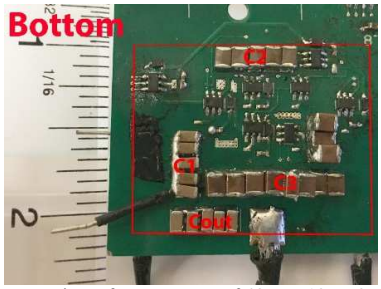

Figure 11: Bottom view of power stage of 48V to 12 V, 35A split-phase Dickson SCC prototype

V. Test Results

Figure 12 shows the efficiency curve obtained from the prototype of the 48-to-12 V, 35A split-phase Dickson SC converter, with the circuit components and configuration as outlined in tables 4 and 5. Figure 13 shows the thermal image of the top side of the prototype during full-load operation.

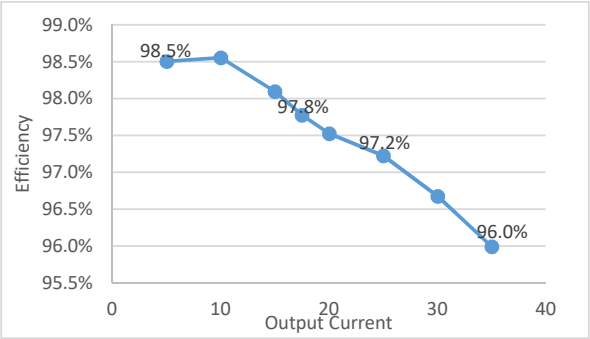

Figure 12: Efficiency Curve for 48V to 12V, 35A Split-Phase Dickson Converter, Initial configuration

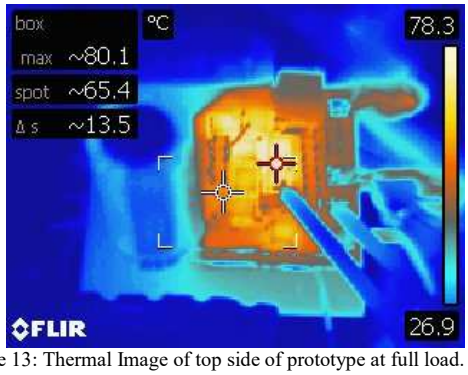

Figure 13: Thermal Image of top side of prototype at full load. Initial configuration

With its circuit components as configured in Tables 3 and 4, the 48 V to 12 V, 35 A prototype attained a peak efficiency of 98.6% at 12V/10A load, and a full-load efficiency of 96% at 12V/35A. A maximum temperature of 80 °C was recorded at full load, with cooling provided by a desk fan.

Figure 14 shows the loss breakdown of the 48V to 12V split-phase Dickson converter at 35 A. The loss breakdown chart shows that the predominant cause of power loss at full load is MOSFET switching loss at 43%, followed by the loss due to the electrolytic input capacitor.

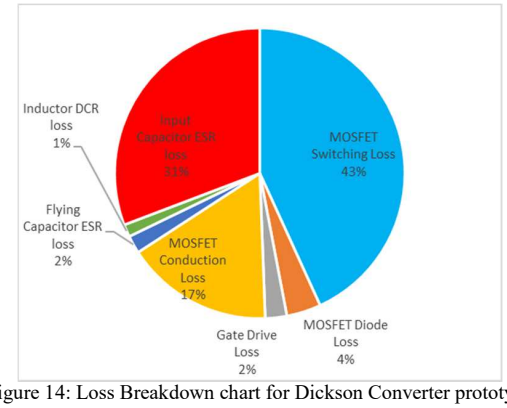

Figure 14: Loss Breakdown chart for Dickson Converter prototype

Figures 15, 16, and 17 show the voltage waveforms for the flying capacitors C1, C2, and C3, respectively, at full load.

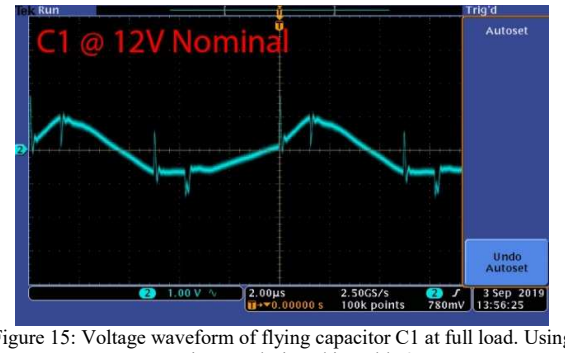

Figure 15: Voltage waveform of flying capacitor C1 at full load. Using capacitors as designed in Table 3.

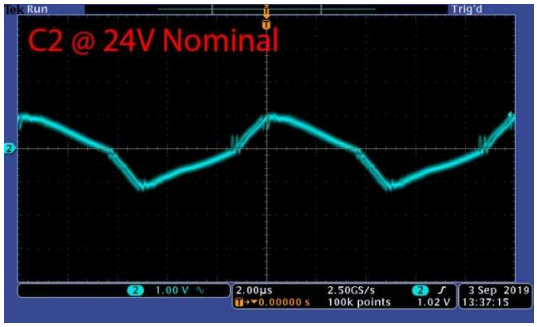

Figure 16: Voltage waveform of flying capacitor C2 at full load. Using capacitors as designed in Table 3.

Figure 17: Voltage waveform of flying capacitor C3 at full load. Using capacitors as designed in Table 3.

To validate the actual values of the prototype's flying capacitors, measurements were performed using the flying capacitors' voltage waveforms to determine the real value of the prototype's flying capacitors. This was accomplished using the in-circuit estimation method outlined in Section IV-A. The flying capacitor sizes as measured under full-load operation are shown in Table 5.

TABLE 5: EXPECTED VS. CALCULATED FLYING CAPACITOR VALUES OF PROTOTYPE (35 A MEASUREMENTS)

Flying Capacitor and total nominal capacitance	Expected voltage de-rating	Expected total capacitance	Real capacitance (Full load measurements)	Actual de-rating
C3=30x4.7µF	-57%	60.6 µF	78.7 µF	-44.2%
C2=10x10 µF	-42%	58 µF	39.2 µF	-60.8%
C1=10x10 µF	-40%	60 µF	54 µF	-46%

A comparison between the actual and expected flying capacitor values in Table 5 shows significant differences between the expected and actual de-rating values of some of the flying capacitors. The most significant anomalies between the measured and expected capacitance values were observed in capacitors C3 and C2. C3 de-rated by around 44% at 36 V during testing, less than the expected 57% derating. C2 de-rated by around 60% at 24 V during testing, significantly more than the expected 42%. C1 de-rated roughly as expected, but its actual de-rating is still slightly larger than its expected de-rating. These measurement results exemplify the variances in capacitance that can result from measurement errors in both the de-rating curves and experimental values, as well as manufacturing tolerance and effects of the actual in-circuit conditions when the capacitors are used in a switching converter. This analysis of actual flying capacitor values show that fine tuning may be necessary to improve the performance of the split-phase Dickson converter, owing to practical limitations of ceramic capacitor de-rating and manufacturing tolerance.

To determine whether matched flying capacitors would result in efficiency improvements, additional ceramic capacitors were added to both C2 and C1 to bring their capacitances closer to the value of C3. 9 capacitors were added to capacitor C2 (for a total of 19 capacitors for C2), while 5 capacitors were added to capacitor C1 (for a total of 15 capacitors for C1). A comparison of efficiency curves between operating the prototype with fully matched flying capacitors and operating the prototype with the flying capacitors as initially designed in Table 3, is shown in Figure 18. Figure 19 shows the thermal image of the top side of the prototype with fully matched flying capacitors during full-load operation.

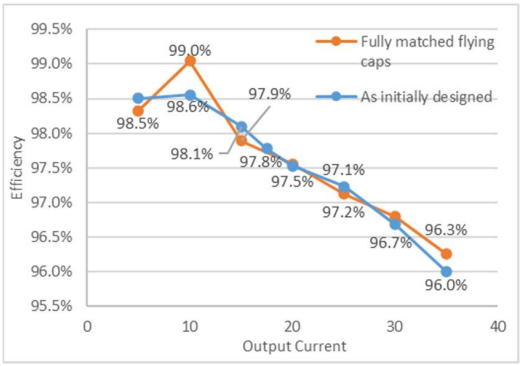

Figure 18: Comparison of efficiency curves for 48 V to 12 V split-phase Dickson converter with fully matched flying capacitors (orange curve) and the prototype with flying capacitors as initially designed in Table 4 (blue curve)

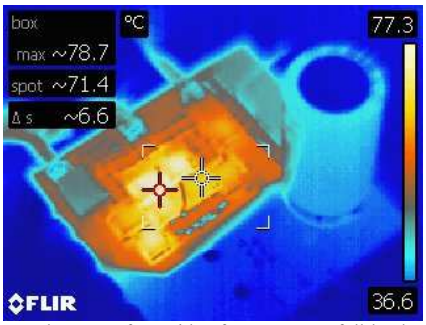

Figure 19: Thermal Image of top side of prototype at full load. Fully matched flying capacitors.

The prototype with tuned flying capacitors saw an overall improvement in efficiency by 0.3-0.4%, with a peak efficiency of 99% at 12V/10A load (versus 98.6%), and a full load efficiency of 96.3% (versus 96.0%) at 12V/35A. The loss reduction between the tuned prototype and the unmodified prototype was 1 W. The tuned prototype experienced a full load power loss of 15 W, down from 16 W experienced by the untuned prototype. Therefore, the loss reduction between the tuned and unmodified prototype was 6.25%. The temperature profile of the prototype has also seen slight improvements, with a maximum temperature of 78.7 °C recorded a full-load operation, as shown in Figure 19.

Therefore, it can be concluded from prototype testing that it is important to ensure that the sizes of flying capacitors of the split-phase Dickson converter are matched as closely as possible, giving consideration that ceramic capacitors de-rate when subjected to a DC voltage bias. This ensures optimal performance of the split-phase Dickson converter.

VI. CONCLUSIONS

The analysis presented in this paper has shown that the split-phase Dickson converter could be successfully adapted for high-current applications of up to 35 A, a level appropriate for data center applications. However, an important design consideration was identified regarding the matching of the circuit's flying capacitors. Because split-phase control relies on charge/discharge control of the flying capacitors to mitigate charge redistribution, uneven charging and discharging due to mismatched flying capacitors results in incomplete

compensation of charge redistribution under split-phase control. To minimize the additional losses caused by charge redistribution, it is crucial that the flying capacitors be designed so that they are matched as closely as possible. To maximize power density and performance, SCCs are generally implemented using ceramic capacitors. However, these capacitors will lose capacitance when subjected to DC voltages, which, combined with typical component tolerances, makes matching the flying capacitors of the split-phase Dickson SCC difficult in practice. Prototype testing has shown that variations in capacitance due to manufacturing tolerance, as well as the possibility of inaccuracies in the supplied capacitor de-rating curves, may require the capacitors of the split-phase Dickson SCC to be tuned to improve their performance. This problem should be addressed for volume production of the split-phase Dickson SCC.

As shown in the loss breakdown chart (Figure 14), a major source of power loss is the input capacitor. The large input capacitor used for the prototype presented in this paper was able to suppress input voltage ripple, however, it decreased the prototype's efficiency. A method to compensate for the effects of input voltage ripple through switch control is currently being developed and tested. This would allow the use of smaller input capacitors, potentially improving efficiency. Furthermore, considering the high switching losses in the split phase prototype, future work may also investigate the possibility of using wide-bandgap devices to reduce the switching losses of the split-phase Dickson converter.

REFERENCES

[1] X. Li and S. Jiang, "Google 48V power architecture," 2017 IEEE Applied Power Electronics Conference and Exposition (APEC), Tampa, FL, 2017, Keynotes presentation

[2] Tianshu Liu, "Novel High Power Density Topologies and Control for the Point-Of-Load (POL) Application," M.A.Sc. Thesis, Department of Electrical and Computer Engineering, Queen's University at Kingston, Kingston, ON, 2016.

[3] D. C. Reusch, "High Frequency, High Power Density Integrated Point of Load and Bus Converters," Ph.D. Dissertation, Virginia Polytechnic Institute and State University, Blackburg, VA, 2012.

[4] V. W. Ng, M. D. Seeman and S. R. Sanders, "Minimum PCB footprint point-of-load DC-DC converter realized with Switched-Capacitor architecture," 2009 IEEE Energy Conversion Congress and Exposition, San Jose, CA, 2009, pp. 1575-1581, doi: 10.1109/ECCE.2009.5316488.

[5] Y. Cao and Z. Ye, "Simulation and analysis of switched capacitor dc-dc converters for use in battery electric vehicles," 2015 IEEE Power and Energy Conference at Illinois (PECI), Champaign, IL, 2015, pp. 1-6, doi: 10.1109/PECI.2015.7064925.

[6] M. S. Makowski and D. Maksimovic, "Performance limits of switched-capacitor DC-DC converters," Proceedings of PESC '95 - Power Electronics Specialist Conference, Atlanta, GA, USA, 1995, pp. 1215-1221 vol.2, doi: 10.1109/PESC.1995.474969.

[7] S. R. Sanders, E. Alon, H. P. Le, M. D. Seeman, M. John, and V. W. Ng, "The Road to Fully Integrated DC-DC Conversion via the Switched-Capacitor Approach," in IEEE Transactions on Power Electronics, vol. 28, no. 9, pp. 4146-4155, 2013.

[8] M. D. Seeman, S. R. Sanders, "Analysis and Optimization of Switched-Capacitor DC-DC Converters," in IEEE Transactions on Power Electronics, vol. 23, no. 2, pp. 841-851, 2008.

[9] M. D. Seeman, "A design methodology for switched-capacitor dcdc converters," Ph.D. dissertation, EECS Department, University of California, Berkeley, May 2009. [Online]. Available: http://www.eecs.berkeley.edu/Pubs/TechRpts/2009/EECS-2009-78.html

[10] V. W.-S. Ng and S. R. Sanders, "Switched Capacitor DC-DC Converter: Superior where the Buck Converter has Dominated," Ph.D. Dissertation, Electrical Engineering and Computer Sciences, University of California at Berkeley, Berkeley, CA, 2011.

[11] Y. Lei and R. C. N. Pilawa-Podgurski, "Analysis of Switched-capacitor DC-DC Converters in Soft-charging Operation," 2013 IEEE 14th Workshop on Control and Modeling for Power Electronics (COMPEL), Salt Lake City, UT, 2013, pp. 1-7, doi: 10.1109/COMPEL.2013.6626416.

[12] Y. Lei and R. C. N. Pilawa-Podgurski, "Soft-charging operation of switched-capacitor DC-DC converters with an inductive load," 2014 IEEE Applied Power Electronics Conference and Exposition - APEC 2014, Fort Worth, TX, 2014, pp. 2112-2119, doi: 10.1109/APEC.2014.6803598.

[13] S. Jiang, S. Saggini, C. Nan, X. Li, C. Chung and M. Yazdani, "Switched Tank Converters," in *IEEE Transactions on Power Electronics*, vol. 34, no. 6, pp. 5048-5062, June 2019.

[14] Y. Lei, Z. Ye and R. C. N. Pilawa-Podgurski, "A GaN-based 97% efficient hybrid switched-capacitor converter with lossless regulation capability," *2015 IEEE Energy Conversion Congress and Exposition (ECCE)*, Montreal, QC, 2015, pp. 4264-4270.

[15] B. B. Macy, Y. Lei and R. C. N. Pilawa-Podgurski, "A 1.2 MHz, 25 V to 100 V GaN-based resonant Dickson switched-capacitor converter with 1011 W/in3 (61.7 kW/L) power density," *2015 IEEE Applied Power Electronics Conference and Exposition (APEC)*, Charlotte, NC, 2015, pp. 1472-1478.

[16] C. K. Tse, S. C. Wong and M. H. L. Chow, "On lossless switched-capacitor power converters," in *IEEE Transactions on Power Electronics*, vol. 10, no. 3, pp. 286-291, May 1995.

[17] Y. Lei, R. May and R. Pilawa-Podgurski, "Split-Phase Control: Achieving Complete Soft-Charging Operation of a Dickson Switched-Capacitor Converter," in *IEEE Transactions on Power Electronics*, vol. 31, no. 1, pp. 770-782, Jan. 2016

[18] D. Gunasekaran and F. Z. Peng, "Design of GaN based ultra-high efficiency, high power density resonant Dickson converter for high voltage step-down ratio," *2019 IEEE Energy Conversion Congress and Exposition (ECCE)*, Baltimore, MD, USA, 2019, pp. 845-852, doi: 10.1109/ECCE.2019.8912960.

[19] O. Jong, Q. Li, F. C. Lee and B. Carpenter, "Loss Model and Optimization Method for Switched-Capacitor Divider for POL Application," *2018 IEEE Energy Conversion Congress and Exposition (ECCE)*, Portland, OR, 2018, pp. 3844-3850, doi: 10.1109/ECCE.2018.8558151.

[20] Q. Li, J. Chen, D. Jiang, "Periodic Variation in the Effect of Switching Frequency on the Harmonics of Power Electronic Converters," in *Chinese Journal of Electrical Engineering*, vol. 6, no. 3, pp. 35-45, September 2020.